JOURNAL OF GEOPHYSICAL RESEARCH, VOL. 94, NO. B4, PAGES 4241–4252, APRIL 10, 1989

Local Versus Global Variations in Ocean Ridge Basalt Composition: A Reply

EMILY M. KLEIN[1] AND CHARLES H. LANGMUIR

Lamont-Doherty Geological Observatory and Department of Geological Sciences of Columbia University, Palisades, New York

INTRODUCTION

Geochemical studies of basalts recovered from individual ridge segments have often identified local chemical diversity and suggested that a component of this diversity results from differing extents of partial melting of the mantle. In some cases, local variations in the extent of melting have been related to tectonic features, such as propagating rift tips [*Christie and Sinton*, 1986], the "cold edge" of the "transform fault effect" [*Bender et al.*, 1984; *Langmuir and Bender*, 1984], or the special environment of seamount formation [*Batiza and Vanko*, 1984]. In other cases, however, as for example in studies of the FAMOUS area, local chemical diversity attributable to melting has not yet been shown to have clear temporal or spatial systematics [e.g., *Langmuir et al.*, 1977; *le Roex et al.* 1981].

The approach of studying the chemical relationships among individual samples from particular ridge segments contrasts with the approach that we adopted in our global study of basalt compositions [*Klein and Langmuir*, 1987] (hereafter referred to as K&L) First, in that study we emphasized the potential of major elements for investigating the extent and pressure of melting of the mantle. Second, we chose to average all chemical data available from a particular region (generally about 100 km of ridge length), in order to minimize the component of local variability and thus to investigate "global" chemical systematics.

The use of averaged data inevitably leads to questions concerning the characteristics of the unaveraged data, and the extent to which the results depend upon the averaging procedure. In their constructive comment to our paper, *Brodholt and Batiza* [this issue] (hereafter referred to as B&B) have presented unaveraged data (i.e., individual analyses) from an independently compiled data base of mid-ocean ridge basalt (MORB) compositions. They show that although the systematics of the individual samples display more scatter than our regional averages, the same overall chemical relationships seen in the averaged data emerge, with the sole exception of the systematics for SiO_2. Furthermore, the data for individual samples also show the same overall relationships between chemistry and depth as are seen in the regionally averaged data. Nonetheless, the figures B&B present show substantial scatter and in themselves suggest that there must be other important processes controlling the chemical variability.

B&B also raise important questions concerning the relationship (if any) between the local and global chemical systematics, and "the length scale of the phenomena responsible for the global systematics." Are the local variations simply the global variations in microcosm? If so, do local axial depth variations of even a few hundred meters reveal small-scale mantle temperature variations? Or do the local and global chemical variations show different systematics that reveal different aspects of the processes involved in creating ocean crust?

The questions raised by B&B provide an impetus to try to understand more clearly the relationship between the local and global variability of MORB compositions. This response addresses that problem. We have found that it is often possible to resolve the chemical variations of MORB into two distinct vectors in composition space. One vector parallels the global array and is best observed in compilations of regional averages; the second vector is clearly expressed in several local arrays of data and is orthogonal to the global array.

In the following discussion, we will (1) respond to the treatment of the data by B&B, (2) present a theoretical argument for the existence of orthogonal local and global trends, (3) present the MORB chemical data showing the existence of the orthogonal local and global vectors, and (4) begin to explore how the distinction between local and global variability may lead to a deeper understanding of the melting process beneath ocean ridges.

RESPONSE TO THE APPROACH OF BRODHOLT AND BATIZA

Regional Averages Versus Individual Analyses

In K&L we showed that regional averages of basalt composition correlate with regional averages of smoothed axial depth and suggested that these global correlations may result from mantle temperature gradients associated with convection. There are both theoretical and practical reasons why these global systematics are best explored with such regional averages, rather than individual sample analyses and their associated depths of recovery.

Large variations in mantle temperature are unlikely to occur over short lateral distances beneath mature ridge axes. Yet, local axial depth variations of more than a thousand meters often occur over less than a few tens of kilometers of ridge length. In addition, studies of local chemical diversity show that relatively large variations in the extent of melting can occur over distances of a few kilometers [e.g., *White and Bryan*, 1977; *Langmuir et al.*, 1977]. Clearly, these local variations in axial depth and extent of melting are unlikely to result from large-scale mantle temperature gradients. From a practical standpoint, a further reason for averaging concerns

[1]Now at Department of Geology, Duke University, Durham, North Carolina.

Paper number 88JB04272.
0148-0227/89/88JB-04272$02.00

the problem of sampling biases. Some ridges are far better sampled than other ridges, and correlations composed of the raw data will be dominated by the better sampled ridge segments. Until such time as all ridge segments are equally well-sampled, regional averaging converts a data set with significant sampling biases into a usable form for exploring the global systematics. Thus there were sound scientific reasons for averaging - averages are more likely to represent the global processes we wished to study.

It is also important to recognize that the concept of a "regional" average differs fundamentally from the averages presented by B&B. In our regional averages, data obtained on individual samples are grouped with respect to locality, whereas the averages of B&B average all data within a given depth window, irrespective of location. Such averages will, for example, eliminate the apparent fine structure within the global correlations, such as the distinct trends seen between different oceans (see for example, Figure 2*d* of K&L). In addition, from a statistical point of view, if the number of raw data points is large, if the data approach a random distribution with respect to the abscissa (depth), and if the window over which the average is taken is small relative to the total variation, the "depth window" averages of B&B will necessarily create smoother trends. Thus these depth window averages reveal little about the nature or scale of global correlations.

The question, therefore, is not whether the global systematics should be investigated by individual analyses and sampling depths, on the one hand, or regional averages of chemistry and depth, on the other: for the reasons just discussed, regional averages represent the more useful approach for studying the global systematics. Instead, the compelling questions raised by B&B concern the relationship between local chemical variability and global chemical variability, and the length scales over which the global and local systematics occur. To address these questions it is necessary to clearly establish the characteristics of the global data set.

Some Considerations of Data Compilation and Treatment

B&B compiled an independent MORB data base for their presentation, and therefore their raw data are not directly comparable to the data base represented by the regional averages of K&L. Although we are in agreement with the general amount of scatter presented in their figures, we also feel the need to point out a few important differences between the two data bases.

In an effort to achieve rigorous impartiality, B&B included all analyses of "zero-age" samples from the references cited, and therefore their compilation contains some analyses with obvious problems. For example, in the compilation of K&L, where information on phenocryst content and state of alteration was presented by the data source, highly phyric and altered samples were excluded. In contrast, the data base of B&B appears to include both highly phyric samples, such as the basaltic gabbros of *Schilling et al.* [1983], and altered samples, such as weathered rocks with over 5 wt % total water [*Humphris et al.*, 1985].

There is in addition an important difference between the depths plotted by B&B and those of K&L. In the compilation of B&B, sample recovery depth is plotted (e.g., dredge depth) while in K&L, we reported an average axial depth for that location, irrespective of the sample recovery depth. This distinction becomes particularly significant for slow-spreading ridges, where "zero-age" samples are often recovered from rift valley walls; for such samples, the reported sampling depth may differ from the "axial depth," and presumably the depth of eruption, by as much as 2000 m. Thus, in a correlation between axial depth and composition, the use of recovery depths can lead to as much as 2000 m of "noise" in the data array of individual samples.

While these factors presumably contribute to the scatter in the B&B plots, they are not the fundamental cause of the scatter. If one takes the standard deviations of the data set presented in Table 1 of K&L and adds error bars of two standard deviations to the global correlations of Figure 2 of that paper, the scatter indicated is similar to that shown in the figures of B&B. It should be recognized, however, that a small number of averages with large standard deviations contribute substantially to the scatter, and these points are typically associated with regions where incompatible element-enriched basalts have been recovered. Nonetheless, the overall level of scatter in the raw data documented by B&B seems to reflect real variability: local variability scatters the global systematics.

The Question of SiO_2

The one result of K&L that B&B were unable to find in the raw data is the correlation between regional averages of SiO_2 and $Na_{8.0}$, and the contrast in SiO_2 between the Pacific and Atlantic oceans, presented in Figure 6 of K&L. B&B conclude that the SiO_2 systematics are simply not present in the individual analyses. Because the range of SiO_2 in MORB is quite small (48 wt % and 52 wt %), it is necessary to pay particular attention to factors that might affect a comparison of data on a global scale. Our previous discussion of SiO_2 relied on a limited data set of high-precision silica analyses of high-MgO glasses, with some attention paid to interlaboratory bias (as noted in the text and caption to Figure 6 in K&L). In order to compare our averaged data with those for individual analyses, the data set of individual analyses must be approached with similar care.

One complicating factor for SiO_2 is the problem of interlaboratory comparison. Figure 1*a* shows SiO_2 analyses of the same sample glasses determined by microprobe at the Smithsonian Institution and by plasma emission spectrometry at Lamont (solid circles). Note that the microprobe analyses are an average of 0.75 wt % higher in SiO_2 than plasma analyses (this difference is 20% of the total range of 4 wt % observed in MORB). Part of the difference between plasma, microprobe and other analytical techniques results from differing methods for reporting iron contents. When the data are renormalized to a comparable basis (open circles), as described in the figure caption, the microprobe data still remain comparatively high. It was for this reason that in Figure 6*b* in K&L, we applied an empirical correction factor of 0.988 to the Smithsonian microprobe SiO_2 data for the mid-Cayman rise in order to plot these data with plasma data from other regions. Note that no such corrections were applied by B&B, and they used data from a large number of laboratories.

A second factor affecting SiO_2 data is the increase in SiO_2 resulting from fractionation of olivine, plagioclase, and clinopyroxene, illustrated in Figure 1*b*. In Figure 6*b* of K&L, we attempted to minimize the effects on SiO_2 due to fractionation by plotting only analyses with 8-10 wt % MgO

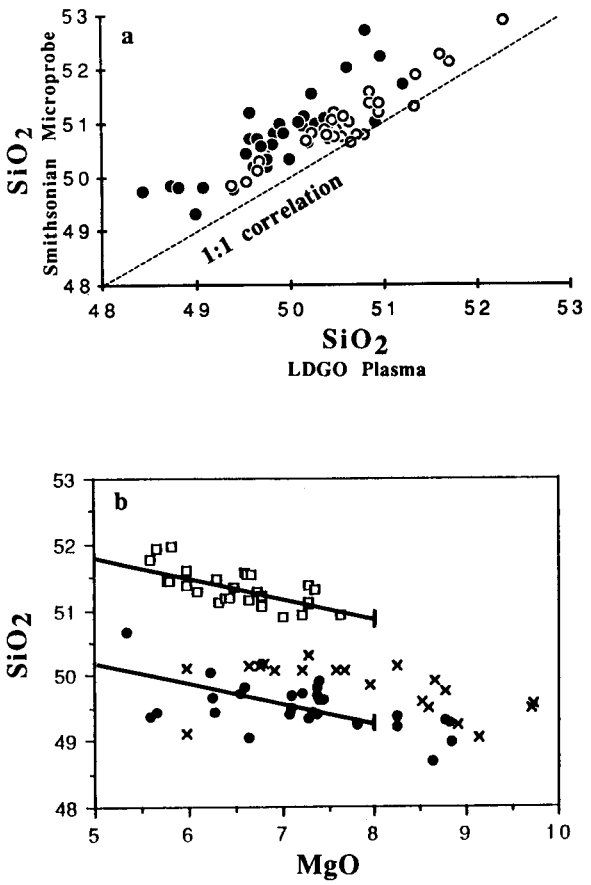

Fig. 1. (*a*) Comparison of SiO_2 abundances determined on the same sample glasses by plasma emission spectrometer at Lamont and by the Smithsonian Institution microprobe. Solid circles show the raw data; open circles show the plasma data recalculated with iron as FeO* and both analytical techniques normalized to sum to 100%. (*b*) MgO versus SiO_2 for three regions (open squares, mid-Cayman rise glasses, Smithsonian Catalog of Basalt Glasses of W. Melson; solid circles, plasma data, East Pacific Rise glasses; crosses, Kolbeinsey Ridge, whole rock powders, [*Schilling et al.*, 1983]. All data have been renormalized as described for Figure 1*a*. Note the greater scatter in the Kolbeinsey Ridge whole rock analyses, compared to the glass data. Lines show the slope of the algorithm used to calculate $Si_{8.0}$ = SiO_2+0.31*MgO-2.48. $Si_{8.0}$ is calculated for samples with 5-8.5 wt % MgO.

(as noted in the text) supplemented by normalized data for the mid-Cayman rise and Kolbeinsey Ridge. This criterion, however, results in the exclusion of data from much of the world, and we have therefore chosen here to adopt the same technique for fractionation-correction that we used for sodium and iron in K&L. Lines showing the slope of the algorithm used to calculate $Si_{8.0}$ are shown in Figure 1*b*, and the equation used for the calculation is given in the figure caption.

In Figure 6*a*, the normalized $Si_{8.0}$ data are plotted versus $Na_{8.0}$ for our compilation of individual samples. In spite of the corrections applied to account for both interlaboratory biases and fractionation, the individual analyses show no apparent correlation between $Si_{8.0}$ and $Na_{8.0}$, supporting the conclusion of B&B. Thus it is a perplexing finding that while regional averages of basalt data show a positive correlation between sodium and silica, the individual analyses show only scatter.

THE RELATIONSHIP BETWEEN GLOBAL AND LOCAL VARIABILITY

We are thus in basic agreement with the observations made by B&B concerning the characteristics of the MORB data base of individual analyses. Although B&B confirm the findings of K&L in the sense that the systematics of the global correlations emerge from the statistics of the unaveraged data, nonetheless, the correlation between silica and sodium disappears, and we are impressed by the relatively large amount of scatter in the unaveraged plots. These are important observations that need to be better understood. Two major questions are raised by the data: (1) Why does local variability add so much scatter to the global correlations? (2) Does this local variability have a characteristic scale length? We can begin to address both of these questions through a theoretical consideration of the process of melt production beneath ocean ridges.

Chemical Variations Within and Between Melting Columns ("Intracolumn" Versus "Intercolumn" Systematics)

A substantial portion of our earlier paper presented the chemical systematics of mantle melting based on experimental data and theoretical considerations. The results, summarized in Table 2 of that paper, showed that for a given source composition, Na_2O is sensitive primarily to the extent of partial melting, while FeO and SiO_2 are sensitive to the pressure of melting as well. FeO increases with increasing pressure and, in upwelling diapirs, decreases as the extent of melting increases. This was shown theoretically by *Langmuir and Hanson* [1980] and can be confirmed using the experimental data of *Jacques and Green* [1980]. The experimental data also show that SiO_2 decreases with increasing pressure.

The puzzle posed by the averaged MORB data was that low-sodium melts have high iron and low silica: that is, the extent of melting seems to correlate positively with the pressure of melting. High-degree melts appear to have equilibrated at higher pressures. A resolution of this problem emerged from a consideration of the effect of pooling melts from throughout "melting columns." In this model, schematically shown in Figure 2, hotter mantle intersects the solidus at greater depth and creates a taller melting column (column X); if melts pool from throughout the column, this would lead to greater mean pressures of melting, as well as greater mean extents of melting. Cooler mantle intersects the solidus at a shallower depth and creates a shorter melting column, leading to lower mean pressures and extents of melting (column Y). Thus in K&L the global systematics of averaged data were explained by variations among different melting columns, or by "intercolumn" variations. This leads to positive correlations between $Na_{8.0}$ and $Si_{8.0}$, and inverse correlations between $Na_{8.0}$ and $Fe_{8.0}$, the relationships that are observed in the global systematics of averaged data and discussed at length in K&L.

We also considered briefly, however, the likely chemical systematics that occur within a single melting column (e.g., Figure 10*a* of K&L), or "intracolumn" variations. Within each melting column, the lower-degree melts are deep, and the higher-degree melts are shallow (Figure 2). In terms of chemical variations, the low-degree melts would have high sodium, high iron, and low silica, while high-degree melts would have low sodium, low iron, and high silica. If local

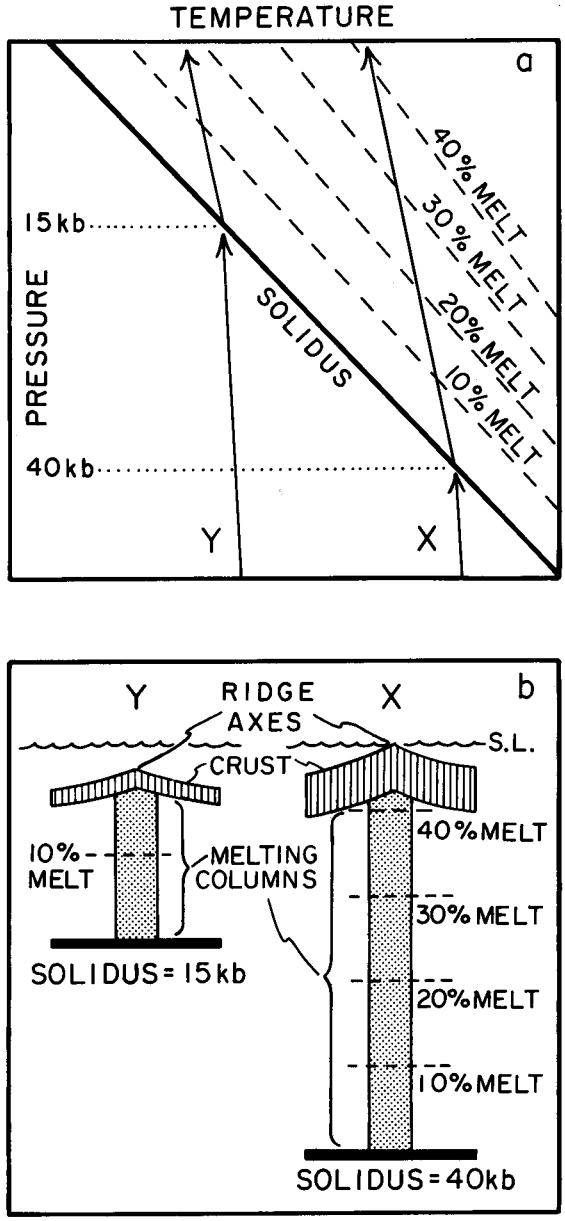

Fig. 2. (*a*) Schematic drawing of mantle pressure versus temperature. Path X represents a hotter parcel of mantle that intersects the solidus at greater depth and undergoes great extents of melting upon ascent; path Y, a cooler parcel of mantle, intersects the solidus at shallower depth and melts less upon ascent. (*b*) Schematic cross section of the oceanic crust and mantle resulting from paths X and Y in Figure 2*a*; light shading indicates the melting column discussed in the text; vertical ruling indicates the oceanic crust.

chemical variations result from the sampling of instantaneous melts from a single melting column, these are the chemical systematics that we would expect to observe along individual ridge segments. Note that these local chemical variations would be opposite to the global chemical systematics. We thus can envision, on theoretical grounds, that the local vector of chemical variability can be orthogonal to the global vector of variability. This clearly could lead to substantial dispersion on plots that use individual data points, because an orthogonal vector of local variability efficiently imparts scatter to the global vector!

Illustration of "Intercolumn" and "Intracolumn" Variations Using Experimental Data

It may help to visualize the contrasting global and local vectors by illustrating them using the experimental data reported by *Jacques and Green* [1980]. (Note that these compositions are not truly experimental liquids, but are calculated from their experimental results. Nonetheless, they remain among the best experimental estimates yet available of the effects of progressive partial melting of the mantle at different pressures.) Figures 3*a* and 3*b* show the SiO_2, FeO*, and Na_2O contents of melts for melting of pyrolite at 2, 5, 10, and 15 kbar. Because Na_2O behaves as a moderately incompatible element during melting, at each pressure of melting, the Na_2O contents of the melts decrease with increasing extents of melting. Also with increasing extents of melting, these and other experimental studies [e.g., *Fujii and Scarfe*, 1985; *Takahashi and Kushiro*, 1983] show a slight increase in SiO_2 abundances and the approximately constant or slight increase in FeO contents. The most dramatic effect on FeO and SiO_2, however, contents results from variations in the pressure of melting. Increased pressures of melting decrease the SiO_2 contents and increase the FeO* contents of the melts.

The results of these experimental studies reveal the changing melt composition with increasing extents of melting at a single pressure. Melting beneath ridge axes, however, is polybaric. The compositional variations resulting from polybaric melting can be estimated from the experimental data if an assumption is made regarding the extent of melting that occurs per kilobar of pressure release above the solidus. As in K&L, we use the value of 1.2% melt per kilobar pressure release.

In Figures 3*c* and 3*d*, two polybaric melting paths based on the melting columns (paths X and Y illustrated in Figure 2) are shown schematically for the Na_2O versus SiO_2 or FeO* data of Jacques and Green. The melting column represented by path X intersects the solidus at 40 kbar and with continued adiabatic upwelling continues to melt to about 5 kbar. If melts pool from throughout this melting column, the mixed melt will have a composition reflecting a high mean pressure and extent of melting; the pooled melt composition for this column is represented by the asterisk along path X. Path Y intersects its solidus at a substantially lower pressure (15 kbar) and continues to melt to about 2 kbar (the final pressure is lower than for path Y due to a decreased crustal thickness). The lower mean pressure and extent of melting for path Y will lead to a pooled melt composition represented by the asterisk along path Y.

The "intercolumn" variations, corresponding to the global correlations of regional averages, are illustrated by the trends formed by the two asterisks in Figures 3*c* and 3*d* (the pooled melt compositions from each melting column) which are located at the mean pressure of melting ($\bar{P}$ of K&L) for each melting column. Column X, which intersected its solidus at greater depth, will have lower mean Na_2O and SiO_2 abundances and higher FeO* abundances than column Y, which intersected its solidus at shallower depth. Thus if the regional averages of the MORB data reflect the mean output from the melting column, we would expect a positive correlation between the Na_2O and SiO_2 contents, and an inverse correlation between Na_2O and FeO* contents of parental magmas from region to region. These are the compositional variations observed

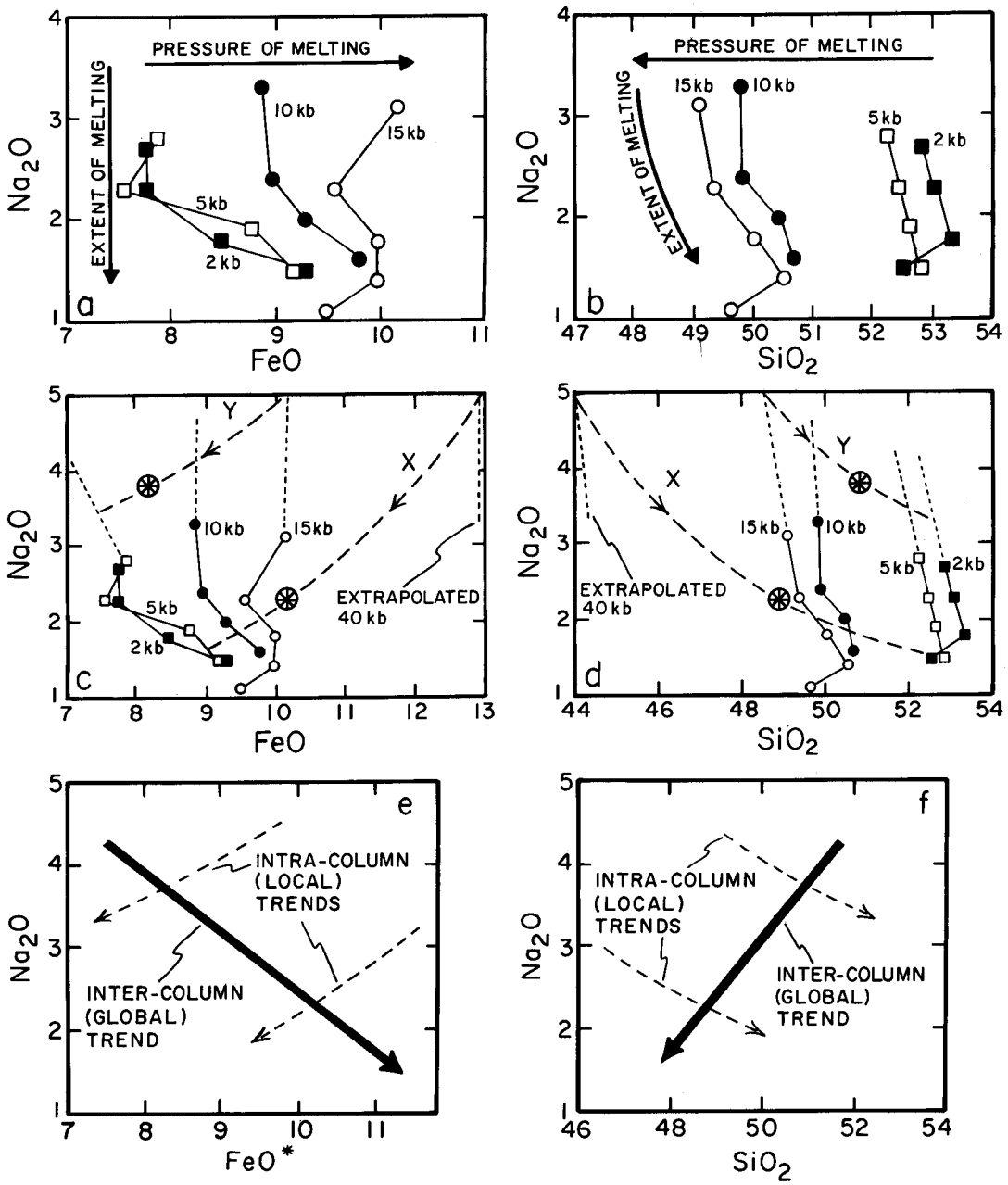

Fig. 3. (*a* and *b*) Data of *Jacques and Green* [1980] for melting of pyrolite at 2, 5, 10, and 15 kbar, showing the effects on melt composition of increasing extents and pressures of melting. (*c* and *d*) Data as in Figures 3*a* and 3*b*; dashed lines show inferred polybaric melting paths for different pressures of intersection of the solidus (X and Y) shown in Figure 2. Circled asterisks indicate approximate compositions of pooled melts for the mean pressure (see *Klein and Langmuir* [1987]) from each melting column. (*e* and *f*) Schematic drawing of relationship between intercolumn (global) and intracolumn (local) chemical trends, adapted from Figures 3*c* and 3*d* and discussed in the text.

among the regional averages of the MORB data presented by K&L.

But the "intracolumn" variations, which one might expect to see in local variability, should have compositional systematics that correspond to the individual paths of X or Y. That is, among samples from an individual ridge segment, low Na_2O would be observed with relatively high SiO_2 and low FeO - systematics that are opposite to those expected for "intercolumn" variations. Thus a suite of melts related to one another by the same pressure of intersection of the solidus (intracolumn), on plots of sodium versus silica or iron, should form correlations of the opposite slope to those formed by the pooled melts (Figures 3*c* and 3*d*). The chemical distinctions between the "intercolumn," or global vector, and the "intracolumn," or local vector, are shown schematically in Figures 3*e* and 3*f*.

Clearly, this way of thinking about melting systematics hinges on the concept of the "melting column." As a physical entity, a vertical melting column as we have presented it here and in K&L is not a physically realistic "shape" for a melting regime beneath an ocean ridge. But a "melting column" is the net effect of virtually all realistic melting regime shapes. This

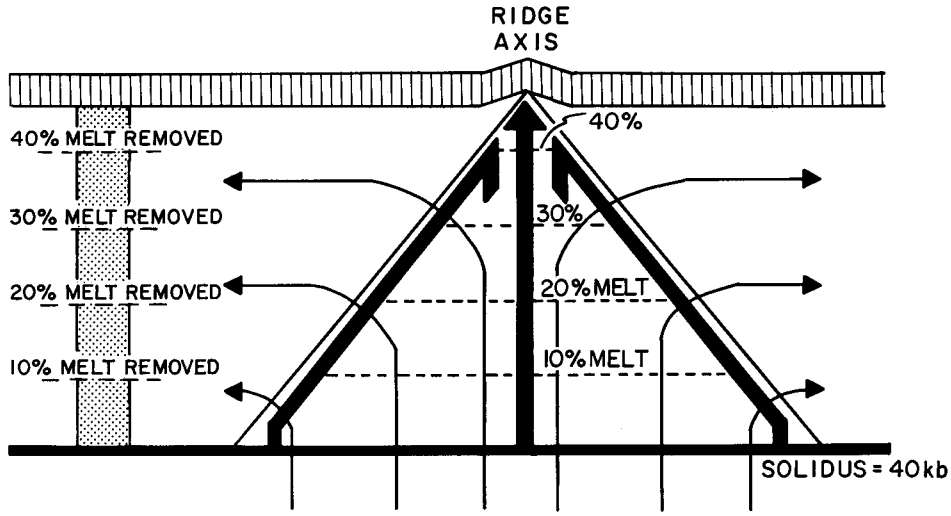

Fig. 4. Schematic model of the melting zone beneath a ridge axis, adapted from *Oxburgh* [1980]. Light solid arrows show paths of upwelling and diverging mantle; heavy solid arrows show melt flow field after *Spiegelmăn and McKenzie* [1987]; dashed lines within melting zone show percent melting above solidus. Oceanic crust is indicated by vertical ruling. Residual melting column resulting from the extraction of melt (stippled) is shown at left.

idea, which is not intuitively obvious, is illustrated in Figure 4. The extent of melting that occurs in a parcel of mantle relates to the extent of pressure release above the mantle solidus that the parcel experiences. Thus for any laminar flow regime of the mantle through a melting zone, the amount of melt produced is controlled by the vertical component of flow. That parcel of mantle that ascends highest, melts most. At the end of the process, if one considers a vertical section extending from the base of the crust to the depth of the mantle solidus, there is a vertical gradient in the amount of melt removed as a function of depth - i.e., a melting column (Figure 4). Thus the concept of a melting column is a reasonable representation of the net result of the melt extraction process beneath ridges. The precise shape of the melting regime, however, may affect the extent to which melts mix and where these melts are likely to be erupted.

LOCAL VERSUS GLOBAL TRENDS AS OBSERVED IN THE MORB DATA BASE

The reasoning presented above can be tested by investigating local variability within the MORB data base. In order to minimize the effects of interlaboratory biases, in the following discussion we have used primarily analyses obtained by three laboratories for which we have information on interlaboratory biases: the Smithsonian microprobe overseen by W. Melson, J. G. Schilling's laboratory at the University of Rhode Island, and our own analyses by plasma emission spectrometry at Lamont. The data set that meets the zero-age and MgO criteria includes over 1000 analyses and represents worldwide coverage. Because the majority of analyses were obtained by the Smithsonian microprobe, we have adjusted all analyses to the Smithsonian microprobe data; information on the empirical corrections applied is given in the caption to Figure 5.

Iron, Silica, and Sodium Variations in MORB

Individual MORB analyses of iron, sodium, and silica, normalized to a constant value of 8 wt % MgO, are shown in Figures 5 and 6 (algorithms for normalization are presented in K&L and herein). These plots of $Fe_{8.0}$ versus $Na_{8.0}$ and $Si_{8.0}$ versus $Na_{8.0}$ are analogous to the plots of experimental data in Figure 3. Individual analyses with no local identification are shown in Figures 5*a* and 6*a*, and confirm the substantial scatter noted by B&B.

In Figures 5*b* and 6*b* the same data are shown, but with samples from six well-sampled local regions in the Atlantic, representing most of the range in regional depth, labeled with separate symbols. The areas are the Reykjanes Peninsula, the FAMOUS-Narrowgate area, the AMAR area, the mid-Atlantic ridge south of the Kane Fracture Zone and between 11.4°N and 12°N, and the mid-Cayman rise. While sampling density varies considerably among these regions, in each case, data exist for more than five sampling sites over less than approximately 60 km; for the FAMOUS-Narrowgate region, there are 75 analyses (solid circles). Note that each of the local arrays defines a trend of similar slope. For both $Fe_{8.0}$-$Na_{8.0}$ and $Si_{8.0}$-$Na_{8.0}$, these slopes define "local" vectors that are consistent with the "intracolumn" effects discussed above. These local trends are of opposite slope to the global (intercolumn) trends of K&L. Examining $Fe_{8.0}$-$Na_{8.0}$ systematics of data between the Moore and Rio Grande Fracture Zones at 26°S in the South Atlantic, *Batiza et al.* [1988] recently and independently also noted systematics in $Fe_{8.0}$ and $Na_{8.0}$ that are opposite to the global trends, and suggested that such local trends may be typical of the Atlantic as a whole.

Thus it appears that the greater scatter observed in the data for individual samples is due, at least in part, to "local" trends that are of opposite slope to the overall "global" trends of the regional averages presented by K&L. Two orthogonal vectors act to create the apparent chaos of Figures 5*a* and 6*a*, as well as the $Na_{8.0}$ versus SiO_2 figure of B&B. Much of the scatter in Figures 5*a* and 6*a* appears to result from a series of local trends, stacked in the direction of the global trend. These local trends are compressed to single points by taking regional averages. Thus it is clear why, in a plot of the regional averages, it is the global trend that emerges.

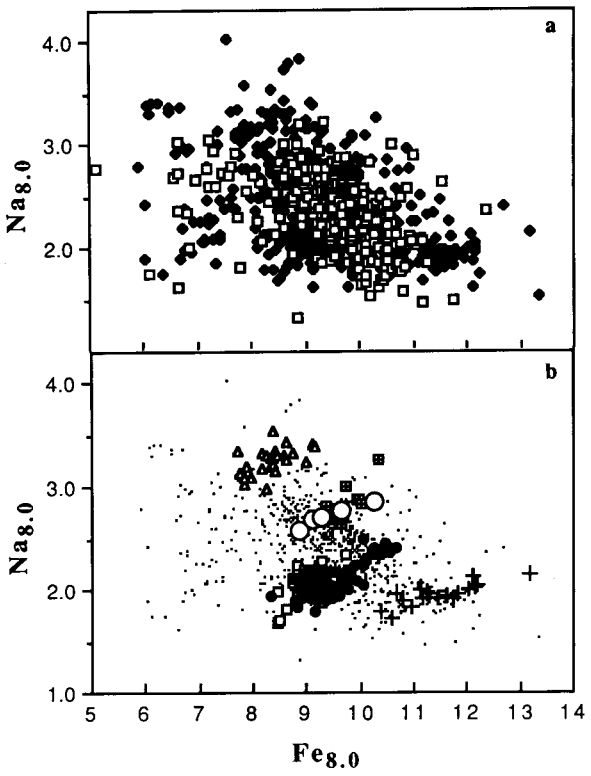

Fig. 5. (a) $Fe_{8.0}$ versus $Na_{8.0}$ (iron and sodium normalized to a constant value of 8 wt % MgO; see *Klein and Langmuir* [1987] for discussion of normalization procedure) for 1050 individual samples analyzed by the Smithsonian microprobe, by *Schilling et al.* [1983] and *Schilling et al.* [1982]; by plasma emission spectrometry at Lamont; and by *Jakobsson et al.* [1978]. Symbols distinguish data from Atlantic and Indian ocean ridges (solid diamonds) and from Pacific ridges (open squares). All data have been recalculated with iron as FeO and renormalized to 100%. In addition, based on our comparison of interlaboratory biases, the following empirical correction factors have been applied to the Lamont, University Rhode Island and Jakobsson data so as to be comparable to the Smithsonian microprobe data: Na_2O, 0.98; MgO, 0.96; SiO_2, 1.006; FeO, 1.025. (*b*) Data from Figure 5*a* shown as small dots, with the data from six regions in the North Atlantic highlighted: Reykjanes Peninsula (crosses); FAMOUS-Narrowgate region (solid circles); AMAR region (open squares); 11.4°N-11.97°N MAR (open circles); MAR south of Kane Fracture Zone (squares with crosses); mid-Cayman rise (open triangles). Note that the raw data from each of the regions highlighted have been examined to evaluate the efficacy of the constant algorithms used to calculate $Na_{8.0}$ and $Fe_{8.0}$; in the following cases, the algorithm has been empirically adjusted to better reflect the liquid line of descent for that region and to ensure that the local trends are not artifacts of the normalization procedure. South of Kane: $Fe_{8.0}$ = 1.056 * MgO + FeO - 8.446; Reykjanes Peninsula: $Na_{8.0}$ = 0.255 * MgO + Na_2O - 2.046; mid-Cayman rise: $Fe_{8.0}$ = 0.924*MgO + FeO - 7.39.

There are two obvious problems that need to be discussed concerning the line of reasoning presented above. The first concerns the fact that the correlations of the regional averages have substantial "fine structure" (such as the low iron of the Azores region). The second concerns the possibility that processes other than the melting systematics discussed above may produce the local vectors.

Fine Structure in the Global Correlations

As we noted in K&L and elsewhere [*Langmuir*, 1987], there is substantial "fine structure" within the global correlations. This is particularly apparent in iron and seems to occur preferentially around some hot spots. In principle, provided we have a representative sample of the melting column, each local data array should be symmetrically disposed over the global trend: that is, the global trend should bisect the local trends. Examination of Figures 5*b* and 6*b* shows, however, that this is not the case for the two hot spot regions that are plotted. The FAMOUS and AMAR data are offset to low $Fe_{8.0}$ and high $Si_{8.0}$, while the Reykjanes Peninsula data are offset to low $Si_{8.0}$ and to a lesser extent high $Fe_{8.0}$. Such offsets are also apparent in the global correlations of regional averages (Figure 2 of K&L). These offsets may reflect very large-scale "intracolumn" effects of hot spots; K&L noted, for example, that variations around hot spots tended to be orthogonal to the global correlations. Alternatively, they may be due to temporal variations in the sampling of melts from a melting column. It is also possible, however, that these offsets of the local trends relative to the global trend reflect major element heterogeneity of the mantle source. If the latter, then there may be no single global correlation in composition space, but rather a global band reflecting variability in mantle sources. Imposed on the structure of this band would be the local vectors for each individual region. Answers to these possibilities will require more detailed sampling of many local regions in the vicinity of hot spots, more information on temporal variability in basalt composition, and detailed experimental data on the effects of major element source heterogeneity on the compositions of mantle melts.

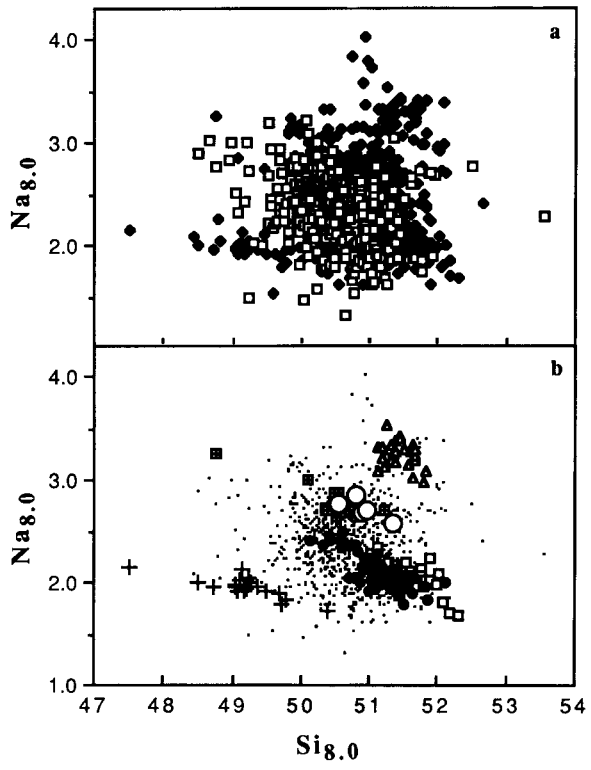

Fig. 6. $Si_{8.0}$ versus $Na_{8.0}$ (see also *Klein and Langmuir* [1987] and caption to Figure 1); data and symbols as in Figure 5.

Other Hypotheses for the Origin of the Local Vector

Although we have posed one hypothesis for the origin of the orthogonal local vector, there are other possibilities that can be considered. For example, the compositional variations of the local trends may result from major element heterogeneity of the mantle, or from the melting of a veined mantle. In the former case, the trends from high iron and sodium to low iron and sodium in the densely sampled regions of the Atlantic may reflect the melting of more fertile to more depleted mantle compositions. Experimental studies on the melting of fertile and depleted peridotites [e.g., *Jacques and Green*, 1980] suggest that for the same extent of melting, a more fertile mantle composition may produce melts that show an association between higher silica and sodium: in contrast, the local trends observed in the Atlantic show an inverse correlation between silica and sodium. More fertile mantle, however, can also be expected to intersect its solidus at greater depth, leading to greater extents and pressures of melting. Thus the relationship between degree of source fertility and the extent and pressure of melting may be complex, and the possibility that the local trends result from mantle heterogeneity cannot be ruled out.

The local trends may also result from high-pressure fractionation [e.g., *Elthon et al.*, 1982; *Elthon and Scarfe*, 1984]. Indeed, qualitatively, high-pressure fractionation of clinopyroxene ± orthopyroxene ± olivine would be expected to produce the associated increase in iron and sodium, and if olivine plays only a minor role, an associated decrease in silica contents of the residual magmas. A quantitative evaluation of this possibility would require detailed knowledge of phase relations and phase compositions over a range of pressures and is beyond the scope of the present discussion.

THE LENGTH SCALE OF CHEMICAL VARIABILITY

The identification of local and global vectors provides insight into the length scales of chemical variability. For that portion of ridge fed by a single melting column, chemical variability will reflect the local subsolidus mantle temperature, local tectonics, mantle and crustal plumbing, small-scale mantle heterogeneity and temporal variability. The "intracolumn" effects can thus be expected to dominate on this scale, and there may be no resolvable regional mantle temperature gradient. Depths on this scale are likely to be controlled by similar processes. But what scale is this? Are there different scales over which the systematics of a single melting column appear to dominate, ranging from a hot spot at one extreme, to a single axial volcano at the other? We can begin to address these questions with basalt chemistry.

The recognition that local variability, whatever its causes, obscures the global systematics, leads one to imagine that if one removed the local vector of variability, then the global systematics might emerge even more clearly. One way to carry out this exercise is to project the local arrays onto the global vectors, as illustrated in Figure 7. This procedure then yields values for each individual data point ($Fe^G_{8.0}$ and $Si^G_{8.0}$ which reflect only the global component of variability. The algorithms used to calculate $Fe^G_{8.0}$ and $Si^G_{8.0}$ are presented in the caption to Figure 7. The extent to which the local trends deviate from the constant algorithm used will introduce error into the calculated $Fe^G_{8.0}$ and $Si^G_{8.0}$ values, and this projection may eliminate meaningful fine structure in the global correlations, such as the asymmetric disposition of the

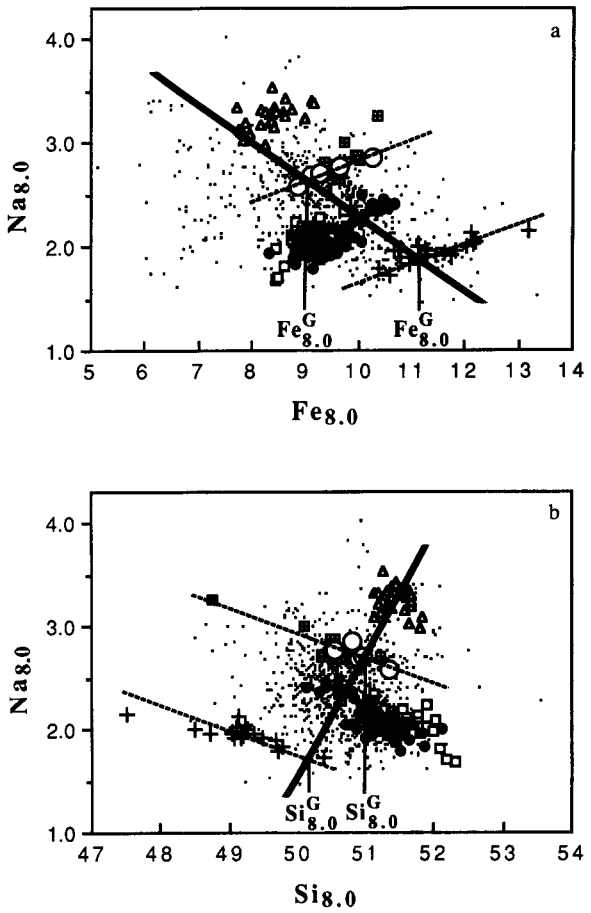

Fig. 7. Same as Figures 5*a* and 6*a*; dashed lines are "local" trends for data from densely sampled individual regions in the North Atlantic; solid lines are "global" trends used for projection, estimated from *Klein and Langmuir* [1987]. $Fe^G_{8.0}$ and $Si^G_{8.0}$ values are calculated as follows: for each individual sample, calculate: $b_{Fe} = Na_{8.0} - 0.19 * Fe_{8.0}$ and $b_{Si} = Na_{8.0} + 0.27 * Si_{8.0}$; then $Fe^G_{8.0} = 2.033 * (5.233 - b_{fe})$ and $Si^G_{8.0} = 0.689 * (b_{si}+57.5)$.

FAMOUS and Reykjanes Peninsula data about the global correlations. Figure 8 shows the relationship of these parameters to depth for the entire data set of individual samples (note that recovery depths have been used for comparison with figures of B&B). The systematic behavior of silica with depth now clearly emerges, and the iron data are better defined.

Although the projection scheme essentially forces the data set as a whole to correlate sodium with iron (Figure 7*a*) and sodium with silica (Figure 7*b*), it does not necessarily follow that $Fe^G_{8.0}$ will correlate with $Si^G_{8.0}$ for individual samples. This nonintuitive result derives from the fact that an individual sample analysis need not project to the same sodium content on each of the two bivariant plots of Figures 7*a* and 7*b*. Consider, for example, a hypothetical situation in which two samples have identical $Fe_{8.0}$ and $Na_{8.0}$ values but very different $Si_{8.0}$ values (i.e., the data show no systematic behavior betweeen silica and sodium or iron). These two samples will obviously project to the same $Fe^G_{8.0}$ and sodium values in Figure 7*a*; however, in Figure 7*b* the two samples will project to different $Si^G_{8.0}$, as well as different sodium values. Thus these samples will show no correlation between $Fe^G_{8.0}$ and $Si^G_{8.0}$. The fact that the real MORB data do indeed

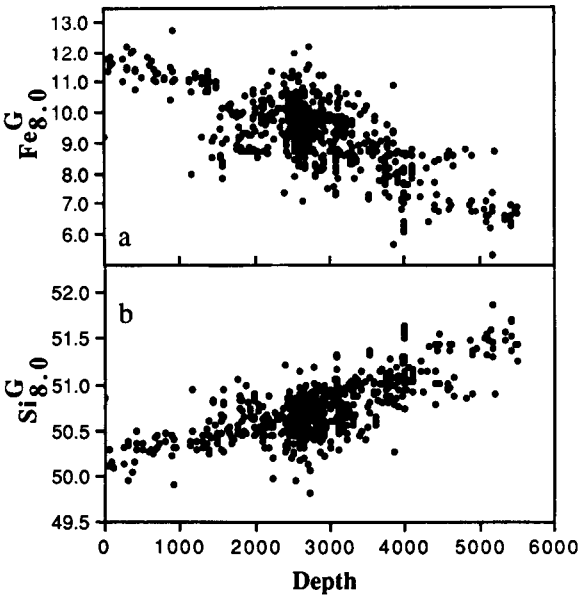

Fig. 8. Sample recovery depth for individual samples versus (*a*) $Fe^G_{8.0}$ and (*b*) $Si^G_{8.0}$. See caption to Figure 7 for algorithms.

show a strong correlation between $Fe^G_{8.0}$ and $Si^G_{8.0}$ (Figure 9) demonstrates, first, that the individual analyses do in general project to similar sodium values in Figures 7*a* and 7*b* and, more importantly, that there is a systematic relationship between silica, iron, and sodium that is described by the local vector. In essence, the correlation of $Fe^G_{8.0}$ with $Si^G_{8.0}$ shows that the original $Na_{8.0}$, $Fe_{8.0}$, and $Si_{8.0}$ data are approximately planar. Indeed, principal components analysis shows that 88% of the $Na_{8.0}$, $Fe_{8.0}$, and $Si_{8.0}$ variability of the 1050 individual MORB samples can be accounted for by two vectors.

The $Fe^G_{8.0}$ and $Si^G_{8.0}$ parameters are quite "processed" since they are first corrected for MgO content and then corrected for local variability. Their potential utility and physical meaning, however, are illustrated by the data for the northern mid-Atlantic ridge. In Figures 10*a* and 10*b* are shown the quite scattered data for $Fe_{8.0}$ and $Si_{8.0}$ versus latitude. Figures 10*c* and 10*d* show that the same analyses calculated as $Fe^G_{8.0}$ and $Si^G_{8.0}$ display much smoother variations as a function of latitude and, in addition, correlate with large-scale bathymetric variations (Figure 10*e*). Note that on the plots of $Fe^G_{8.0}$ and $Si^G_{8.0}$ both Iceland and the Azores emerge as hot regions, although some variability in $Fe^G_{8.0}$ is seen in the latter. In addition, some fracture zones, such as Gibbs and Jan Mayen Fracture Zones, coincide with abrupt changes in composition (temperature?), while the Kane Fracture Zone appears to form an inflection point. Thus if the $Fe^G_{8.0}$ and $Si^G_{8.0}$ values do indeed represent more precise measures of relative differences in mantle temperature, examination of the data for the North Atlantic reveals that discernable mantle temperature variations are often gradational over a thousand kilometers or more, and that some fracture zones coincide with major changes in the temperature beneath the adjacent, offset ridge axes.

In regard to the question raised by B&B concerning the length scale of mantle temperature variations, it is useful to examine regions that show a strong chemical gradient. In Figure 11, the data for the region between 5°N and 35°N in the Atlantic are shown in detail. The available $Fe^G_{8.0}$ data appear to form a dome shape between 5°N and the Kane Fracture Zone, whereas from Kane toward the Azores, the $Fe^G_{8.0}$ values climb dramatically. It is important to note that the strong gradient north of Kane would not be apparent if the data from this region were examined on a significantly smaller scale; examination of the data within a 100-km window, for example, would reveal only scatter. Thus it appears that even in regions that exhibit a strong gradient in $Fe^G_{8.0}$ values, discernable variations in $Fe^G_{8.0}$ and, by extension, in mantle temperature, occur on a scale of >100 km.

THE PACIFIC PUZZLE

Although local trends consistent with "intracolumn" chemical variations emerge clearly in the Atlantic data, the same is not true of Pacific data. On a plot of $Fe_{8.0}$-$Na_{8.0}$ (Figure 12*a*), data from densely sampled segments of the East Pacific Rise and Juan de Fuca Ridge either fall along the global trend or show no systematic variations. Although weak inverse trends are seen in the $Si_{8.0}$-$Na_{8.0}$ data for a few regions from the East Pacific Rise (Figure 12*b*), in general the Pacific data show little evidence of the local systematics seen in the Atlantic. Indeed, along some segments of the East Pacific Rise, inverse correlations for both $Na_{8.0}$-$Si_{8.0}$ and $Fe_{8.0}$-$Na_{8.0}$ are observed. Remarkably, data from over 15 sampling sites between the 9°03'N Overlapping Spreading Center and the Clipperton Transform display almost no discernible $Fe_{8.0}$, $Na_{8.0}$, or $Si_{8.0}$ variations (Figures 12*a* and 12*b*). In regard to local systematics of Indian Ocean ridges, it remains uncertain whether the local trends of the Atlantic are present in the Indian Ocean, due to the absence of available major element data for densely sampled Indian Ocean ridge segments.

The contrast between the local systematics in the Atlantic and Pacific is puzzling, but it also raises an interesting question concerning a possible correlation with spreading rate. One of the curious features of the global correlations is the absence of a relationship to spreading rate, suggesting that spreading is a passive phenomenon that is independent of mantle temperature. Local variability, however, may reflect the physical characteristics of the melting zone and the way melts are sampled from it, both of which may indeed be spreading rate-dependent. Thus a better understanding of the local systematics as a function of spreading rate may be a tool for investigating differences in the physical aspects of the melting process beneath slow- and fast-spreading ridges.

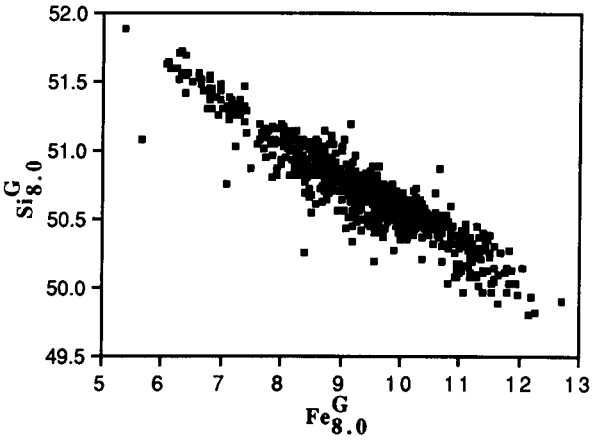

Fig. 9. $Fe^G_{8.0}$ versus $Si^G_{8.0}$. See caption to Figure 7 for algorithms.

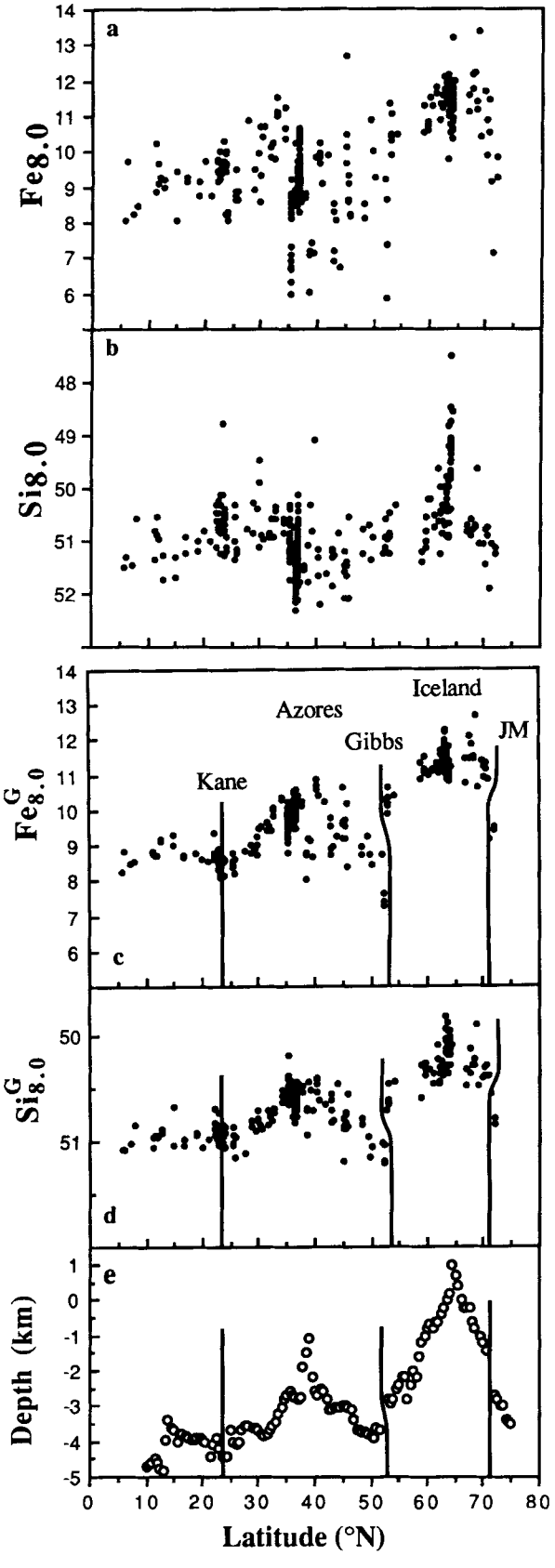

Fig. 10. Data for the North Atlantic: (*a*) $Fe_{8.0}$, (*b*) $Si_{8.0}$, (*c*) $Fe^{G}_{8.0}$, and (*d*) $Si^{G}_{8.0}$. Note that scales for silica parameters are reversed. (*e*) Latitudinal variations in axial depth, taken at 0.5° intervals, from *LeDouaran and Francheteau* [1981] and *Vogt* [1986]. See *Klein and Langmuir* [1987], and captions to Figures 1 and 7 for algorithms.

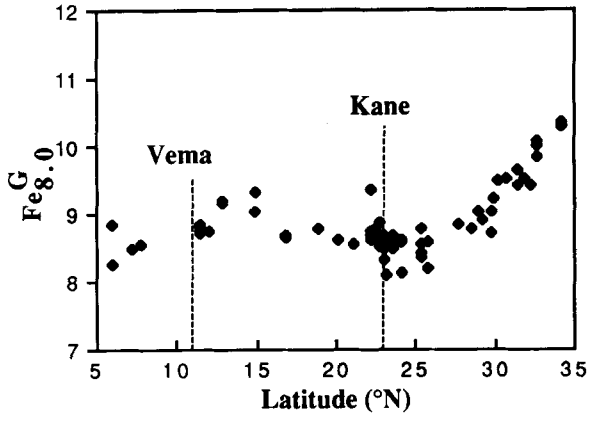

Fig. 11. Detail from Figure 10 of region between 5°N and 35°N along the mid-Atlantic Ridge.

There is one last aspect of the contrast between the Atlantic and Pacific data to be addressed. K&L reported that for the same $Na_{8.0}$ content, regional averages of silica are approximately 0.5 wt % lower in samples from Pacific Ocean ridges compared to those from the Atlantic and Indian Oceans. Examining the raw data for silica, B&B found no evidence of this offset. As shown in Figure 6*a*, considerable overlap exists among the data for the three ocean ridge systems. Nevertheless, although Atlantic and Pacific ocean ridges have almost identical mean $Na_{8.0}$ values (2.34±0.34 and 2.35±0.30, respectively), Pacific ridges have a lower mean $Si_{8.0}$ value of 50.46±0.53, compared to 50.89±0.66 for the Atlantic ridges. Mean $Na_{8.0}$ and $Si_{8.0}$ values for Indian Ocean ridge samples are 2.78±0.38 and 50.84±0.7. Thus we would argue that the present data set, which is of greater global coverage than the limited plasma data for silica previously published as regional averages, supports the subtle distinction in silica between the Pacific and other ridge systems.

CONCLUSIONS

1. Prompted by the work of *Brodholt and Batiza* [this issue], we have resolved the chemical variations of a global data base consisting of individual analyses of mid-ocean ridge basalts into two components, a global component and a local component. The latter was not explicitly addressed in our previous examination of worldwide variations in MORB composition [*Klein and Langmuir*, 1987]. The distinction between the two components is most clearly expressed in data from the Atlantic.

2. Theoretical considerations of the melting process beneath ocean ridges suggest that the global vector of chemical variability may reflect regional differences in the pressure of intersection of the mantle solidus, and therefore in subsolidus mantle temperature [*Klein and Langmuir*, 1987]. In contrast, the local vector of chemical variability may result from the sampling of instantaneous melts from throughout a melting column and therefore may potentially reflect the processes of melt extraction and mixing. Other possible causes of the local vector of chemical variability, such as major element source heterogeneity or high-pressure fractionation, however, cannot be ruled out.

3. By identifying the two orthogonal vectors in the

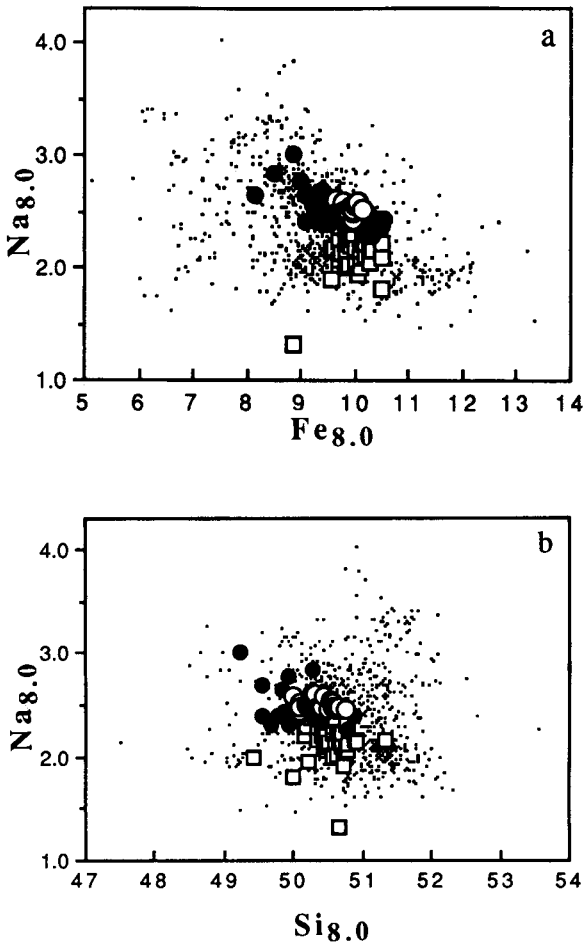

Fig. 12. (*a*) $Fe_{8.0}$ versus $Na_{8.0}$ and (*b*) $Si_{8.0}$ versus $Na_{8.0}$; global data (small dots) as in Figures 5*a* and 6*a*. Larger symbols show data from Pacific ridges. Data from Clipperton transform to 11°45'N Overlapping Spreading Center (solid circles), from Clipperton to the 9°03'N Overlapping Spreading Center (open circles) and from the Juan de Fuca ridge (open squares). Data for East Pacific Rise from C. H. Langmuir and J. F. Bender (personal communication, 1988), and for Juan de Fuca primarily from E. Kappel and C. H. Langmuir (personal communication, 1988).

Atlantic data, it becomes possible to address the important question raised by Brodholt and Batiza concerning the scale of mantle temperature variations. When the effects of the local compositional vector are removed, iron and silica data from the North Atlantic show long-wavelength variations with latitude that correlate with long-wavelength bathymetry, suggesting that mantle temperature gradients can be gradiational over 1000 km or more. Some fracture zones, however, appear to coincide with changes in the temperature of the mantle beneath the adjacent, offset ridge axes. Examination of the data from regions exhibiting strong chemical gradients, such as north of the Kane Fracture Zone, suggests that discernable temperature changes occur over a length scale of greater than 100 km.

4. While the local and global vectors of chemical variability are apparent in the Atlantic, the Pacific data show little evidence of distinct local and global trends. This finding may reflect the influence of spreading rate on physical aspects of melting and melt segregation.

Acknowledgments. We are indebted to J. Brodholt and R. Batiza for providing the impetus to examine the global MORB data base from the perspective of local variability. We also wish to thank D. Walker, A. LeHuray, F. Frey, J. Reynolds, T. Plank, and N. Bogen for their constructive comments. This work was supported by National Science Foundation grants OCE 86-15866, OCE 88-01304 and OCE 84-11448. Lamont-Doherty Geological Observatory Contribution 4416.

REFERENCES

Batiza, R., and D. Vanko, Petrology of young Pacific seamounts, *J. Geophys. Res., 89*, 11235-11260, 1984.

Batiza, R., W. G. Melson, and T. O'Hearn, Simple magma supply geometry inferred beneath a segment of the Mid-Atlantic Ridge, *Nature, 335*, 428-431, 1988.

Bender, J. F., C. H. Langmuir, and G. N. Hanson, Petrogenesis of basalt glasses from the Tamayo region, East Pacific Rise, *J. Petrol., 25*, 213-254, 1984.

Brodholt, J. P., and R. Batiza, Global systematics of unaveraged MORB compositions: Comment on "Global correlations of ocean ridge basalt chemistry with axial depth and crustal thickness" by E. M. Klein and C. H. Langmuir, *J. Geophys. Res.*, this issue.

Christie, D. M., and J. M. Sinton, Major element constraints on melting, differentation and mixing of magmas from the Galapagos 95.5°W propagating rift system, *Contrib. Mineral. Petrol., 94*, 274-288, 1986.

Elthon, D., and C. M. Scarfe, High-pressure phase equilibria of a high-magnesia basalt and the genesis of primary oceanic basalts, *Am. Mineral. 69*, 1-15, 1984.

Elthon, D., J. F. Casey, and S. Komor, Mineral chemistry of ultramafic cumulates for the North Arm Mountain massif of the Bay of Islands ophiolite: Evidence for high pressure crystal fractionation of oceanic basalts, *J. Geophys. Res., 87*, 8717-8734, 1982.

Fujii, T., and C. M. Scarfe, Composition of liquids coexisting with spinel lherzolite at 10 kbar and the genesis of MORBs, *Contrib. Mineral. Petrol., 90*, 18-28, 1985.

Humphris, S. E., G. Thompson, J.-G. Schilling, and R.H. Kingsley, Petrological and geochemical variations along the Mid-Atlantic Ridge between 46°S and 32°S: Influence of the Tristan de Cunha mantle plume, *Geochim. Cosmochim. Acta, 49*, 1445-1464, 1985.

Jacques, A. L., and D. H. Green, Anhydrous melting of peridotite at 0-15 kb pressure and the genesis of tholeiitic basalts, *Contrib. Mineral. Petrol., 73*, 287-310, 1980.

Jakobsson, S. P., J. Jonsson, and F. Shido, Petrology of the western Reykjanes Peninsula, Iceland, *J. Petrol., 19*, 669-705, 1978.

Klein, E. M. and C. H. Langmuir, Global correlations of ocean ridge basalt chemistry with axial depth and crustal thickness, *J. Geophys. Res., 92*, 8089-8115, 1987.

Langmuir, C. H., Testing the relationship between MORB chemistry and axial depth: New data from the Mid-Atlantic ridge between the Kane and Hayes fracture zones, *Eos Trans. AGU, 68*, 1540, 1987.

Langmuir, C. H., and J. F. Bender, The geochemistry of oceanic basalts in the vicinity of transform faults: Observations and implications, *Earth Planet. Sci. Lett., 69*, 107-127, 1984.

Langmuir, C. H., and G. N. Hanson, An evaluation of major element heterogeneity in the mantle sources of basalts, *Philos. Trans. R. Soc. London, Ser. A, 297*, 383-407, 1980.

Langmuir, C. H., J. F. Bender, A. E. Bence, G. N. Hanson, and S. R. Taylor, Petrogenesis of basalts from the FAMOUS area: Mid-Atlantic Ridge, *Earth Planet. Sci. Lett., 36*, 133-156, 1977.

LeDouaran, S. L., and J. Francheteau, Axial depth anomalies from 10 to 50° north along the Mid-Atlantic ridge: Correlation with other mantle properties, *Earth Planet. Sci. Lett., 54*, 29-47, 1981.

le Roex, A. P., A. J. Erlank, and H. D. Needham, Geochemical and mineralogical evidence for the occurrence of at least three distinct magma types in the 'Famous' region, *Contrib. Mineral. Petrol., 77*, 24-37, 1981.

Oxburgh, E. R., Heat flow and magma genesis, in *Physics of Magmatic Processes*, edited by R. B. Hargraves, pp. 161-199, Princeton University Press, Princeton, N. J., 1980.

Schilling, J.-G., R. H. Kingsley, and J. D. Devine, Galapagos hotspot-spreading center system, 1. Spatial petrologic and geochemical variations, 83°W-101°W, *J. Geophys. Res., 87*, 5593-5610, 1982.

Schilling, J.-G., M. Zajac, R. Evans, T. Johnston, W. White, J. D.

Devine, and R. Kingsley, Petrologic and geochemical variations along the Mid-Atlantic Ridge from 29°N to 73°N, *Am. J. Sci., 283*, 510-586, 1983.

Spiegelman, M., and D. McKenzie, Simple 2-D models for melt extraction at mid-ocean ridges and island arcs, *Earth Planet. Sci. Lett., 83*, 137-152, 1987.

Takahashi, E., and I. Kushiro, Melting of a dry peridotite at high pressures and basalt magma genesis, *Am. Mineral., 68*, 859-879, 1983.

Vogt, P. R., Portrait of a plate boundary: The Mid-Atlantic ridge axis from the equator to Siberia, in *The Geology of North America*, vol. M, *The Western North Atlantic Region*, edited by P. R. Vogt and B. E. Tucholke, plate 8A, Geological Society of America, Boulder, Colo., 1986.

White, W. M., and W. B. Bryan, Sr-isotope, K, Rb, Cs, Sr, Ba, and rare-earth geochemistry of basalts from the FAMOUS area, *Geol. Soc. Am. Bull., 88*, 571-576, 1977.

E. M. Klein, Department of Geology, Duke University, Durham, NC 27708.

C. H. Langmuir, Lamont-Doherty Geological Observatory, Palisades, NY 10964.

(Received November 29, 1988;
accepted November 30, 1988.)